EVALUATION OF TRUE STRESS IN ENGINEERING MATERIALS USING OPTICAL DEFORMATION MEASUREMENT METHODS

Paweł Bogusz, Arkadiusz Popławski, Andrzej Morka, Tadeusz Niezgoda

Military University of Technology
Department of Mechanics and Applied Computer Science
Gen. Sylwestra Kaliskiego Street 2, 00-908 Warsaw, Poland
tel.: +48 22 6839941, +48 22 6837610, +48 22 6839461, fax: +48 22 6839355
e-mail: pbogusz@wat.edu.pl, apoplawski@wat.edu.pl,
amorka@wat.edu.pl, tniezgoda@wat.edu.pl

Abstract

The aim of the paper is to evaluate a method of determining true stress in the steel sample subjected to static axial tensile on a universal testing machine. The tensile specimens were made of steel ST3, which was chosen because of its relatively high plastic deformations. Strain measurement was performed using traditional extensometers and additionally a non-contact optical deformation measuring system. Material properties were obtain by the extensometer measurements. The optical equipment registered the investigated sample through the optical system composed of two cameras and calculated a three-dimensional model of the material deformation in time. Displacement fields in axial and radial directions were determined with Digital Image Correlation method (DIC). Then the logarithmic axial strain map and radius shrinkage map in the area of the neck were obtained. Characteristic dimensions of the neck: curvature and width were also measured. It allowed determination of cross-section area changes in the real time, and in the result, calculation of actual true stress in the material during failure process. In this case Bridgman's and other scientists' formulas of stress distribution in the neck were applied. A numerical model, where material properties of finite elements were described by the Johnson-Cooke material model, was developed in LS-PrePost software. The FEM model was computed in LS-DYNA solver. The output tensile curve and neck curvature radius were compared with relevant data obtained from the optical measuring system.

Keywords: true stress, optical deformation measurement, experimental studies, FEM, steel

1. Introduction

In the paper, an axial static tensile test of a metal specimen with high plasticity was conjugated with optical deformation measuring method. Curvature and characteristic dimensions of the neck were measured and true stress as function of true strain in necking area was obtained. Next, Finite Elements Method (FEM) analysis was carried out based on true stress-true strain curve obtained from optical measurement system. Axial true stress as a function of logarithmic strain measured directly by load cell and optical system were compared to the same curve evaluated from the numerical model.

The main tool describing properties of material during strength test is a tensile curve, which is created based on engineering stress as a function of engineering strain. Engineering stress is computed from force readings, which are related to the area of cross-section of the sample measured before the test. Materials with clear yielding stress tend to plasticize when reaching a yielding point. In the last stage of the tensile the neck is created randomly in the measuring area of the sample, what causes reduction of sample cross-section area and a high level of deformation. A standard engineering formula takes into account only the initial dimensions of the specimen and does not consider their changes during the test, thus it can be applied with good accuracy only until the moment of necking. After reaching this stage, the complex stress state develops at the shrinking cross-section of the neck of the tensile specimen.

Many authors proposed theories to solve the problem of the stress distribution in this state. The

first scientist who described successfully the phenomena and deduced the adequate formula was Bridgman [2]. Later Siebel [3], Davidenkov and Spiridonova [4], Szczepiński [5], Petrosian and Malinin [6], and also Vazhentsev [12], proposed their versions of the formula. Their equations are presented in material strength and plasticity theory handbooks.

After spreading of FEM software, computer programs were use to evaluate and improve assumptions and relevance of theoretical formulas [7-11]. Despite questioned accuracy, Bridgman's equation is the most commonly used, especially in western literature. In eastern papers, Davidenkov-Spiridonova equation is the most common [1]. There are also many solutions based on combined experimental-numerical investigations [1, 13].

There are many difficulties in real time deformation measurement with standard tools. Strain gauges and extensometers are the most common, traditional measuring devices. Strain gauges measure local deformation in a given point in the measuring surface area, however, it is very difficult to predict the point of yielding and the necking area. They also have a limited measuring range. Extensometers cannot measure local deformations, however, they measure averaged strain in their base area usually equal to about 20 mm.

Evaluating true stress in the specimen after necking with classic equations, proposed by the above mentioned authors, usually requires knowledge of curvature of the neck and its width. Many authors [13-19], including Bridgman, noticed the difficulty in carrying out those measurements with sufficient accuracy.

The optical measuring system manages to overpass the described drawbacks. The system can measure both local and global deformations of the measuring area of the specimen. Curvature of the neck and width changes in time can be easily obtained with the optical system engaged. Next, after applying adequate formulas to stress distribution, the true stress curve as a function of logarithmic strains can be calculated. Logarithmic strains are more relevant in case of high strains which occur in the necking area of the specimen than engineering strains [1].

In the literature circular cross-section specimens are most commonly analysed as they have better accordance with theoretical assumptions. In some cases rectangular sheet specimens are considered and stress distribution equations are proposed [2, 13]. Author's own investigations showed that the results for circular specimens are more accurate.

2. Specimen description and investigation method

The objective of interest is a cylindrical metal tensile specimen made of ST3 steel. The measuring length is 75 mm and a diameter of the measuring area is equal to 15 mm. The scheme of the specimen is presented in Fig. 1.

The front surface of the specimen was prepared for non-contact optical deformation measurements. Preparation of the specimen required the surface to be coloured white. Next, the specimen was sprayed with a random pattern of black spots, which enabled optical system to identify each fragments of the specimen (facets).
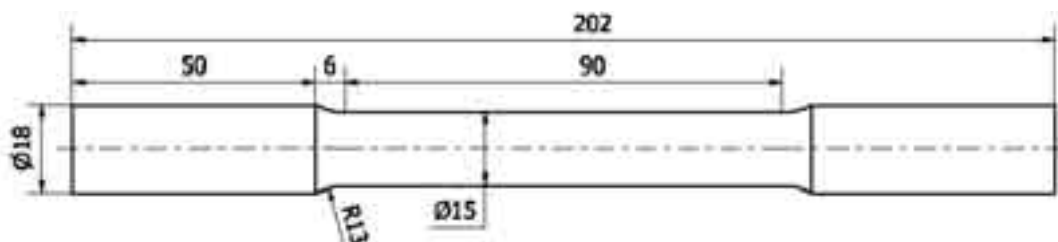

Fig. 1. Scheme and overall dimensions of the tensile specimen

Static axial tension tests were performed on a universal hydraulic tension machine Instron 8802. The specimens were stretched at the constant loading rate equal to 10 mm/min. Loading

force and displacement of the moving head were measured and recorded with the sample rate equal to 20 Hz.

The strain field in measuring area of the specimens (especially in necking area) was detected with the usage of Aramis system. Aramis is a non-contact optical system for measurement of complex materials and structures for their 3D deformation and strain during loading. This tool, equipped with two high-resolution digital CCD cameras (2358x1728 pixels) and 50 mm lens, measures deformation of the investigating specimens during loading, using 3D image correlation methods (DIC – digital image correlation). Due to special specimen surface preparation, the system splits images into rectangular areas called facets which are correlated with the corresponding areas on the other frames.

The system was calibrated with 90x72 mm calibrating plate and recorded 1 picture per second. Based on the recorded pictures, axial strain and radial strain tensors were computed locally in each facet (sized 18x18 pixels which gives 0.45x0.45 mm).

Additionally, longitudinal extensometer Instron model 2620-604 and transverse extensometer Instron model W-E404-E with ±0.5 mm travel were installed on the specimen to investigate an engineering tensile curve and mechanical properties of the material. The measuring base of the longitudinal extensometer was equal to 25 mm. The diametral extensometer measuring base was equal to the specimen initial diameter. The longitudinal extensometer measured engineering axial strain and the transverse extensometer measured diameter shrinkage.

A complete testing system for strength measurements adapted for optical deformation measurements was presented in Fig. 2.
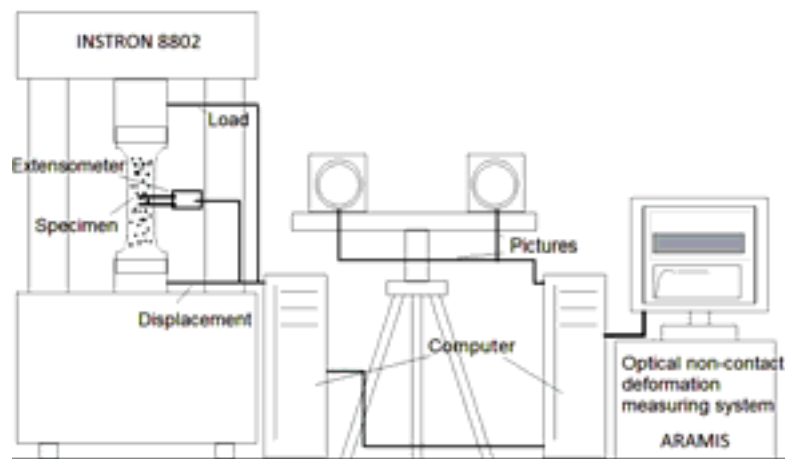

Fig. 2. Scheme of the testing platform adapted for optical deformation measurements

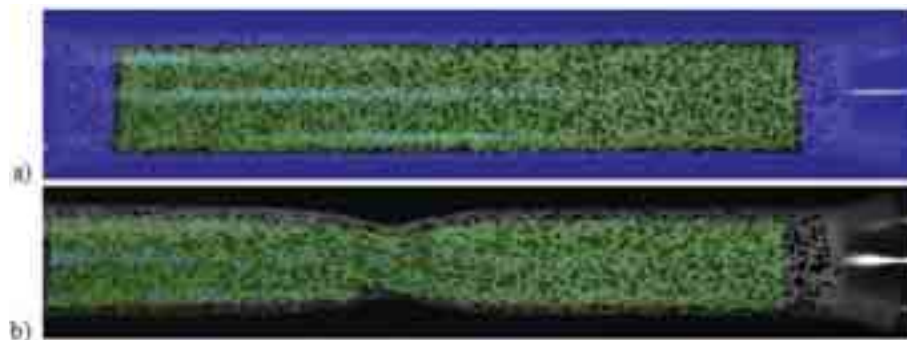## 3. True stress analysis method

Fig. 3. Picture of the specimen taken by optical system with analysed area marked in green: a) on the beginning of the test and b) one frame before failure

Figure 3 presents the specimen as it was pictured by the optical measuring system. Within the analysed area marked green, local strains in facets were measured. Fig. 3 a) presents the unload specimen at the beginning of the test and Fig. 3 b) presents image of the specimen one frame before failure occurred.

Based on the pictures taken by the Aramis system, local axial strains and local radial strains which occurred in the plasticised area of the neck were obtained. Coloured maps of axial logarithmic strains and maps of radius differences for the test stage corresponding to the photo taken one frame before failure (Fig. 3b) are presented in Fig. 8 and 9.

To investigate the region of necking, a stripe of facets within the green region where necking occurred was marked. Picture 4 presents a stripe running through the cross-section, in the middle of the failure point. To obtain a stress-strain curve describing the neck area, local logarithmic axial strains and local radius differences were averaged in this region.

Fig. 4. Fragments of analysed area of specimen marked in the point of failure

Local logarithmic strains are obtained from the formula:

$$\varepsilon_{\log} = \log \lambda, \tag{1}$$

where lambda value is equal to:

$$\lambda = \lim_{l \to 0} \frac{l_0 + \Delta l}{l_0}. \tag{2}$$

Symbol l_0 states for initial distance between two neighbouring facets and Δl is the distance increase during the test.

In the case of the extensometers placed on the specimen, classic engineering strains, both axial and radial, were determined:

$$\varepsilon_{eng} = \lambda - 1. \tag{3}$$

Engineering stress is evaluated in relation to the initial cross-section area:

$$\sigma_{eng} = \frac{P}{A_0}, \tag{4}$$

where:
P – actual force measured by the Instron machine,
A_0 – initial cross-section of a specimen.
Initial cross-section area equals to:

$$A_0 = \pi r_0^2, \tag{5}$$

where:
r_0 – initial specimen diameter.
Average true axial stress $\overline{\sigma}_z$ represents average stress in reference to the lowest actual cross-section in the neck A caused by force P:

$$\overline{\sigma}_z = \frac{P}{A}. \tag{6}$$

Actual neck cross-section area equals to:

$$A = \pi(r_0 + \Delta r)^2 , \tag{7}$$

where:

Δr – actual radius difference measured by the optical system (negative value).

Taking (7) into (6) we have:

$$\overline{\sigma}_z = \frac{P}{\pi(r_0 + \Delta r)^2} . \tag{8}$$

The curve $\overline{\sigma}_z$ can be obtained directly from the performed tensile test. Force is measured by tensile machine and the cross-section area can be acquired from optical measurement results. FEM analysis requires a different true stress-true strain curve:

$$\overline{k} = f(\overline{\varepsilon}^{pl}) , \tag{9}$$

to proceed the simulation.

True stress, in this context, means average intensity of plastic stress [1]. This value incorporates three components of the stress: axial radial and circumferential. True strain is intensity of logarithmic strain and is described by the initial radius to actual radius ratio with the following formula [1]:

$$\overline{\varepsilon}^{pl} = 2\ln\left(\frac{r_0}{r}\right) . \tag{10}$$

The equations linking experimentally measurable curve $\overline{\sigma}_z$ with intensity of plastic stress $\overline{k}$ are described by formulas introduced by Brigdman and other scientists.

In [1] authors studied relative errors for different relationships describing stress distribution in the neck area: Bridgman's (11), Siebel's, Davidenkov-Spiridonova's, Szczepinski's (12), Malinin-Petrosjan's as well as authors' own empirically-numerical equation (13) and its variations. Error of curvature radius obtained from the formulas and numerically calculated was studied. Three types of material were considered relatively to a strengthening type: linear strengthened, nonlinear strengthened and with ideal plasticity one. Tab. 1 presents averaged relative errors of evaluated types of materials when a particular equation is used.

Tab. 1. Comparison of relative errors caused by methods used for determining strengthening curve [1]

Methodology	Linear strengthening	Nonlinear strengthening	Ideal plasticity
	[%]	[%]	[%]
Bridgman (11)	-5.1	-4.2	-10.5
Siebel / Davidenkov-Spiridonova	-2.0	-2.6	-3.8
Szczepinski (12)	2.2	-0.7	6.3
Malinin-Petrosjan	-0.5	-1.7	-2.9
Empirical equation (14)	1.2	-0.3	0.9
Empirical equation (13) with α =0.5 and β = 0.5	-0.5	-1.5	-1.6

A nonlinear model of plastic deformation was assumed according to the investigated specimen on the basis of the $\overline{\sigma}_z$ function – Fig. 6. Based on the error analysis, Bridgman's equation is the method with the greatest error, but it is the most frequently used equation for a neck deformation description [1]. In the case of nonlinear plasticity model, classic Szczepinski equation and empiric equation introduced in [1] have both error factor lower than 1% (Tab. 1). Those three methods were selected to obtain true stress-true strain curves which are presented in Fig. 3.

Bridgman's method is described by the equation:

$$\overline{k}_{Br} = \frac{\overline{\sigma}_z}{\left(1 + \frac{2R}{a}\right)\ln\left(1 + \frac{a}{2R}\right)}. \tag{11}$$

where:
a – is a half of width of the neck in its thinest point,
R – is curvature of the neck.

Width of the neck *2a* and its curvature *R* were measured in Aramis system.

Szczepinski formula has the following form:

$$\overline{k}_{Sz} = \frac{\overline{\sigma}_z}{\frac{2R}{a}\left[\exp\left(\frac{a}{2R}\right) - 1\right]}. \tag{12}$$

In [1] equation:

$$\overline{k}_{Emp} = \frac{\overline{\sigma}_z}{\left[1 + \frac{a}{4R} + \frac{a(1-\beta)\alpha}{R(4-\alpha)}\right]}, \tag{13}$$

was introduced and is dependent not only on *a/R* ratio but also on parameters α and β, which both should be established from numerical simulations [1]. This equation is more generalised form of Siebel equation. In one of its versions, parameter α was equal to 0.95 and $\beta = 0.5$ [1], so that:

$$\overline{k}_{Emp} = \frac{\overline{\sigma}_z}{\left[1 + \frac{a}{4R} + \frac{19a}{488R}\right]}. \tag{14}$$

In the other version of equation (13) parameters $\alpha = 0.5$ and $\beta = 0.5$ were proposed. They can be adjusted by FEM analysis on the basis of neck curvature comparison between experimental and numerical data [1].

Among other assumptions, the assumption about equality of radial strain and circumferential strain in the thinnest cross-section is always made in theoretical analysis:

$$\sigma_r = \sigma_\theta, \tag{15}$$

The same formula is with the strains:

$$\varepsilon_r = \varepsilon_\theta. \tag{16}$$

Index *r* stands for radial dimension and index θ stands for circumferential dimension in both equations.

A to *R* ratio is measurement essential to obtain true stress from equations (11-14). Fig. 5 presents a closer look into strain distribution in the neck area and shows characteristic dimensions of the neck measurement methodology. Curvature radius *R* and width *2a* were measured.
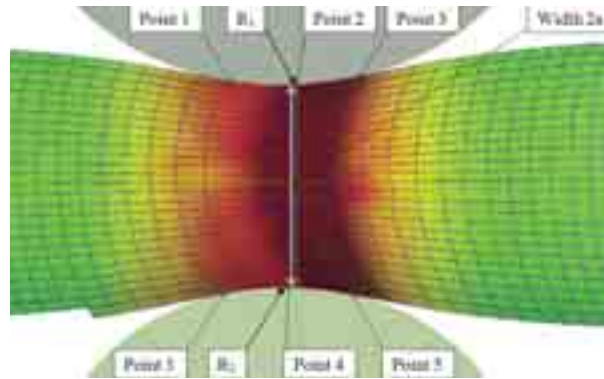
Fig. 5. Curvature radius and width of the neck measurement

Curvature radiuses on both sides of the neck were constructed with usage of two circles built based on the points located on both sides of the neck in its centre area (Fig. 5). The radii were added and average value *R* was taken to calculate *a/R* ratio. Based on two points located on the middle of the neck (Point 2 and 4), the width of the neck on its thinnest diameter was measured (Fig. 9).

Despite very different forms of the equations (11, 12, 14), adequate normalised true stress curves (red, green and violet lines) are very similar to each other, as it can be observed in Fig. 6. The empirical curve of effective stress (14), which is claimed to be the most effective [1], due to the lowest relative error for nonlinear strengthening materials (Tab. 1) was used in FEM calculations.
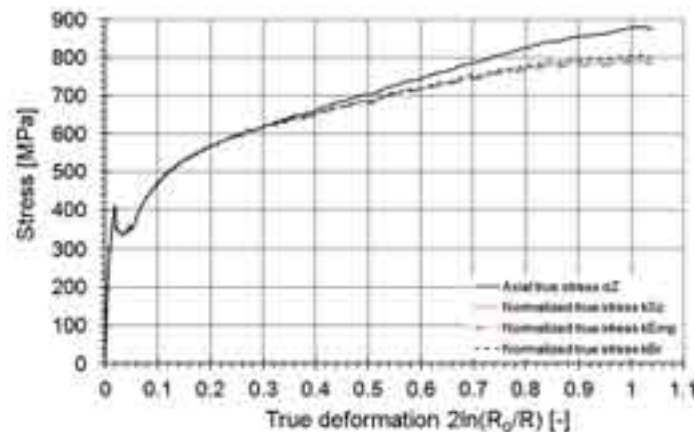

Fig. 6. True axial stress curve compared with obtained normalised true stress curves

Standard engineering methods were used to obtain such material properties of the specimen as: strength, elastic modulus, Poisson's ratio and high low yield point, low yield point, failure strain and relative elongation. All the strength properties are gathered in Tab. 1 and were set in numerical simulations.

Tab. 2. Results obtained from extensometer measurements

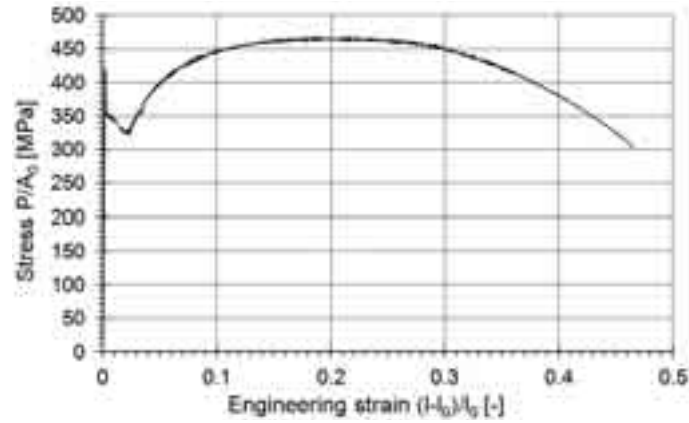| Description	Maximal force	Strength	Elastic modulus	High yield point	Low yield point	Relative elongation	Failure strain	Poisson's ratio
	[kN]	[MPa]	[GPa]	[MPa]	[MPa]	[%]	[%]	[-]
Steel_1	81.33	467.0	211.1	411.0	350.0	40.7	46.5	0.30

Fig. 7. Tensile engineering stress-engineering strain curve

An engineering stress-engineering strain curve is presented in Fig. 7. A high value of plastic deformation of the specimen is clearly visible.

A map of logarithmic local strains in the axial direction measured by optical system before failure is presented in Fig. 8. The highest value was measured in the area of necking and is equal to 81.9%. It correspond to 125.2% engineering strain.

Logarithmic strain in radius direction and actual minimal cross-section area *A* were obtained based on the map of local radius differences measured by the optical system before failure. The map of the deformation of radius is shown in Fig. 9. The highest radius shrinkage measured in the neck area was equal to 2.48 mm.
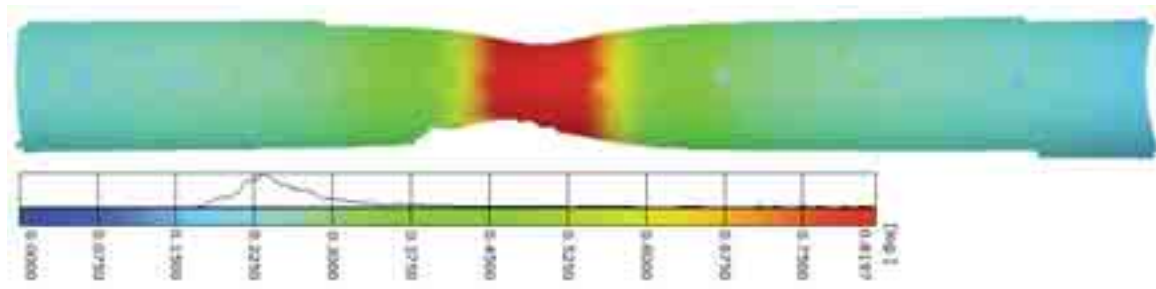

Fig. 8. Map of local logarithmic strains in axial direction measured by optical system before failure
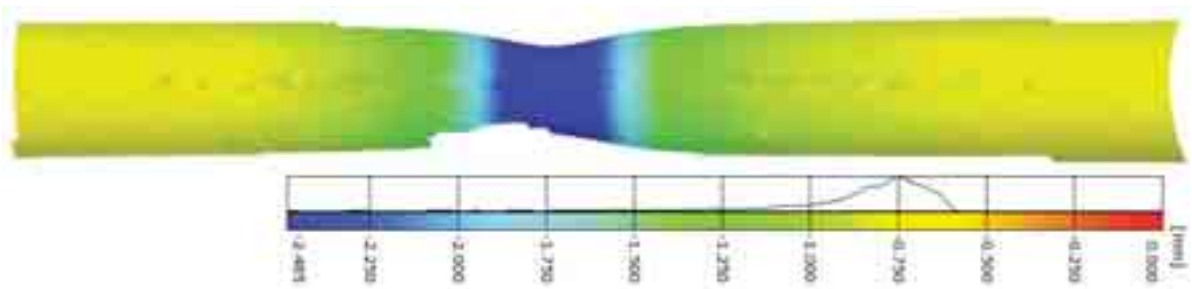

Fig. 9. Map of local radius differences across the specimen measured by optical system before failure

4. Numerical simulations and comparison

After evaluating the data from the experimental test, the curve $\bar{k}_{Emp}$ was introduced and put into the LS-Dyna software along with material properties presented in Tab. 1. Tabulated Johnson Cook Model 224 with solid elements was developed. The model gives ability to describe given material based on effective stress-effective strain curve and material strength properties.

In LCK1 parameter, the given $\bar{k} = f(\bar{\varepsilon}^{pl})$ load curve defines effective stress as a function of effective plastic strain. Mass density RO (7.86 E-3 [g/mm^3]), Young's modulus E, Poisson's ratio PR were taken from experimental data. Failure flag FAIL was called to determine failure moment. The highest failure strain taken from optical measurements (Fig. 8), was input into the Add Erosion model as a Maximum Effective Strain at Failure. All other parameters were set to their defaults [20, 21].

To obtain better adjustment of FEM simulation with experimental results, three types of grid dimensions were tested. In the first model cubic mesh grid dimension was equal to 1.0 mm (faster calculations), in the second model mesh dimension was equal to 0.7 mm and in the third - 0.5 mm (better compatibility with optical facet dimension). Facet dimension in optical measurements was equal to 0.45 mm.

The FEM axial true stress curves $\bar{\sigma}_z$ were obtained in the identical way as in the case of experimental investigations. A stripe of mesh grids in the area of the thinnest neck cross-section was marked. It is important to take similar stripe width as in case of the optical measurements did. Then, averaged true axial stress as a function of effective strain for selected region of mesh was obtained and compared with an equivalent curve obtained from the experimental test. On the Fig. 10 comparison of $\bar{\sigma}_z$ curves from optical analysis and numerical simulation is presented. Dotted green line presents $\bar{\sigma}_z$ from the model with 1.0 mm mesh, long dashed violet line shows $\bar{\sigma}_z$ from the model with 0.7 mm mesh and dashed red line corresponds to curve obtained from the model with 0.5 mm grid. Black solid line is developed from experimental results. Blue line is normalised true stress $\bar{k}_{Emp}$ (14) equal to $\bar{k}$. Abscissa axis presents true deformation calculated from (10).

The model with grid size 1.0 mm has slightly better fit to the experimental $\bar{\sigma}_z$ data than 0.5 mm mesh model, even though mesh size was two times higher than facet size. The 0.7 mm mesh model has the best fit with experimental line in the centre part of the curve (0.4-0.7 true strain range), but the differences are not very significant. The equation (14) is empirically-numerical formula and to obtain better fit of the data parameters α and β in (14) can be adjusted [1].
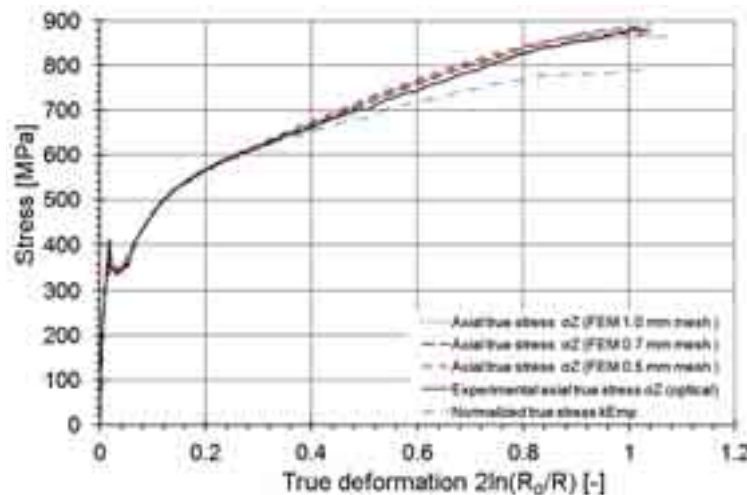

Fig. 10. Comparison of true axial stress obtained experimentally and numerically

Neck curvature radius, which describes the accuracy of plastic deformation modelling, was also evaluated in the similar way as in the case of optical measurements. On the Fig. 11 comparison of the neck curvatures of three models and the specimen is presented. Dotted green line is from the model with 1.0 mm mesh and long dashed violet line is from the model with 0.7 mm mesh. The 0.5 mm mesh model results are presented as dashed red line. Black points represent the results from the experiment.
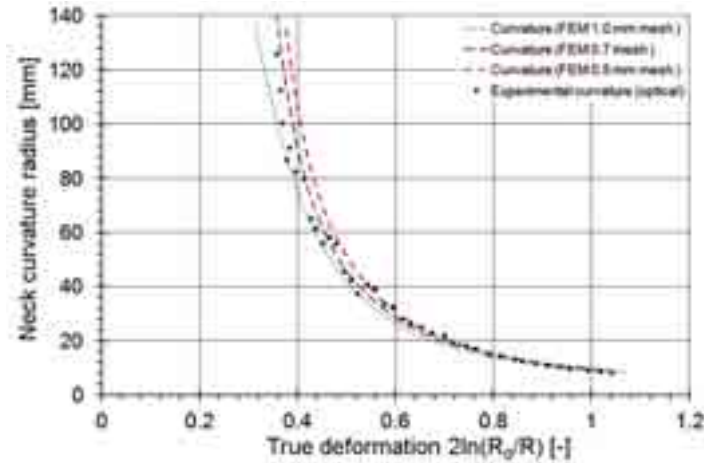
Fig. 11. Comparison of neck curvature from experimental measurements and numerical calculations

It is difficult to measure curvature with optical system with radius 40 mm or greater and higher scatter of results is observed in this area. However, this fragment of the curve corresponds to very first stage of the neck development. In later phase experimentally measured radius results are less scattered.

Results obtain in the FEM simulations with 0.5 mm mesh are similar to the experimental points for 0.5 strain and above. Before this point the curve is too steep. 1.0 mm mesh diverge from experimental points in the first stage of the necking and in the centre part of the curve (0.5-0.6 strain range) inaccurately reflects curvature shape in the thinnest cross-section of the neck. The best overall accuracy with experimental data has 0.7 mm mesh model. It does not diverge as 0.5 mm model in the first stage and fits better in the centre part of the data than 1.0 mm model. This leads to the conclusion that FEM model accuracy of neck plastic deformation modelling depends on the FEM mesh size and can be adjusted by this parameter.

Optical method can measure neck characteristic dimensions with enough precision to be used in numerical simulations. It is important to know that in case of Aramis system only curvature near specimen edge, not on the edge precisely can be measured, due to the system limitations.

FEM simulation results corresponding to the point of failure for the case of 0.7 mm mesh, which has better overall accordance of curvature radius and effective stress fit in the middle stage, comparing to the experimental data, are presented in Fig. 12 and 13. Fig. 12 presents map of effective strain in the neck area from FEM analysis. Maximum effective strain is equal to 1.19. At this stage maximum effective stress is equal to 788 MPa (Fig. 13) and is obtained in the centre of the cross-section of the neck.
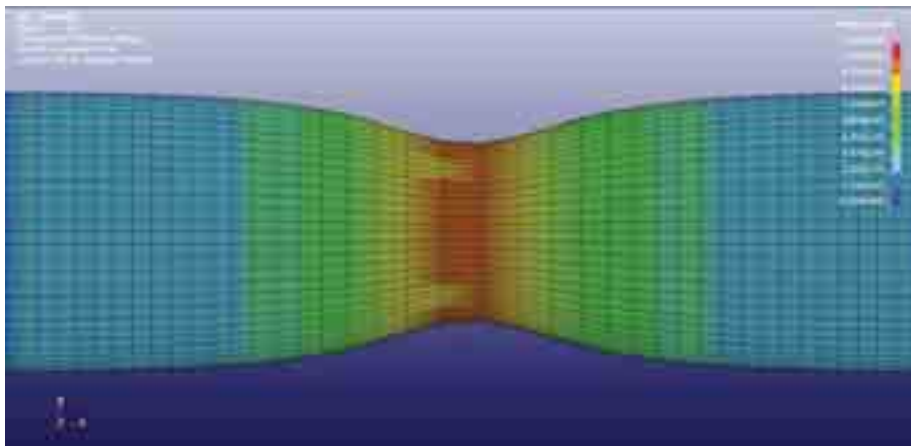

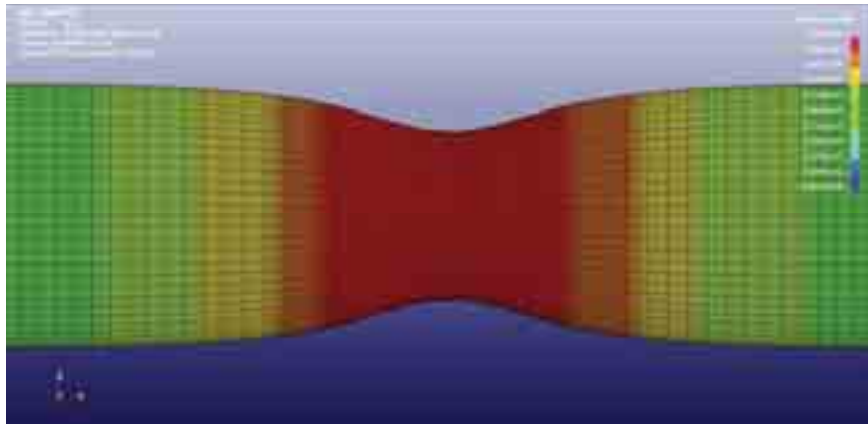*Fig. 12. Map of effective strain in the neck area from FEM analysis*

Fig. 13. Map of effective stress in the neck area from FEM analysis

5. Conclusion

Based on the presented results the following conclusions were derived:
– Optical system is a good tool in the case of true stress-strain curve evaluation. Three dimensional strain maps of a investigated element, both logarithmic and engineering, can be obtained. This enables to investigate specimen cross-section change thru time, in any given point at the specimen measuring area and consequently, actual true axial stress (6) curve can be calculated,
– Optical system can be used to measure characteristic dimensions of the neck. These data manage to evaluate intensity stress from equations (11-14) or others, where fundamental is *a/R* ration and true axial stress knowledge,
– $\bar{k}$ curves obtained from considered stress distribution models differ very slightly to each other (Fig. 6). The empirical equation (14) were used, as it has the lowest curvature error factor. To obtain better fit of the data parameters *α* and *β* can be adjusted or other stress distribution equation applied in case of different characteristics of a material.
– Johnson Cook Model 224 described evaluated material based on effective stress-strain curve $\bar{k}$ and strength properties obtained through experimental test. Good accordance of axial true stress (Fig. 10) and shape of the neck (Fig. 11) were achieved in case of 0.7 mm mesh FEM model. It has the best accuracy in the middle stage of necking.
– Grid dimension plays an important role to obtain better plastic deformation accuracy with this model. The best overall fit with experimental data has 0.7 mm mesh model. It does not diverge as 0.5 mm model in the first stage and fits better in the centre part of the data than 1.0 mm model. The differences between the FEM lines are not significant and the choice of the one depends on which fragment of the necking is the most important to be better reflected for further analysis. Also time of analysis can be important. The 0.5 mm mesh model is calculated quite a long time.

References

[1] Gromada, M., Miszuris, G., *Evaluation of the flow curve in the tensile test and stress distribution in the minimal cross-section*, Oficyna Wydawnicza Politechniki Rzeszowskiej, Rzeszów 2010.
[2] Bridgman, P. W., *Studies in large plastic flow and fracture: with special emphasis on the effects of hydrostatic pressure*, Harvard University Press, Cambridge 1964.
[3] Siebel, E., Schwaigerer, S., Zur Mechanik des Zugversuchs, Archiv für das Eisenhüttenwesen, Vol. 19, pp. 145-52, 1948.

[4]   Davidenkov, N. N., Spiridonova, N. I., *Mechanical methods of testing. Analysis of the state of stress in neck of a tension test specimen*, American Society for Testing and Materials, Vol. 46, pp. 1147-1158, 1947.

[5]   Dietrich, L., Miastkowski, J., Szczepiński, W., *Nośność graniczna elementów konstrukcji*, PWN, Warsaw 1970.

[6]   Malinin, N. N., Rżysko, J., *Mechanika materiałów*, PWN, Warsaw 1981.

[7]   Chen, W. H., *Necking of a bar*, International Journal of Solids and Structures, Vol. 7, pp. 685-717, 1971.

[8]   Needleman, A., *A numerical study of necking in circular cylindrical bars*, Journal of the Mechanics and Physics of Solids, Vol. 20, pp. 111-127, 1972.

[9]   Norris, D. M., Morgan, Jr. B., Scudder, J. K., Quinones, D. F., *A computer simulations of the tension test*, Journal of the Mechanics and Physics of Solids, Vol. 26, pp. 1-19, 1978.

[10] Saje, M., *Necking of a cylindrical bar in tension*, International Journal of Solids and Structures, Vol. 15, pp. 731-742, 1979.

[11] Zhang, K. S., Zheng, C. Q., *Analysis of large deformation and fracture of axisymmetric tensile specimens*, Engineering fracture mechanics, Vol 39, pp. 851-857, 1991.

[12] Vazhentzev, Yu. G., Isaev, V. V., *Problem of the stress state in the neck of cylindrical and flat specimens in tensile loading*, Strength of Materials, Vol. 20, No. 4, pp. 495-499, 1988.

[13] Cabezas, E. E., Celentano, D. J., *Experimental and numerical analysis of the tensile test using sheet specimens*, Finite element in analysis and design, Vol. 40, pp. 555-575, 2004.

[14] Gabryszewski, Z., Gronostajski, J., *Mechanika procesów obróbki pastycznej*, PWN, Warsaw 1970.

[15] Jasieński, Z., *Wpływ nierównomierności odkształcenia na zależność naprężenia właściwego od stopnia deformacji w szycje rozciąganej próbki metalowej*, Archiwum Hutnictwa, Vol. 10, pp. 189-239, 1965.

[16] Ling, Y., *Uniaxial true stress-strain after necking*, AMP Journal of Technology, Vol. 5, pp. 37-48, 1996.

[17] Szczepiński, W., *Metody doświadczalne mechaniki ciała stałego*, PWN, Warszawa 1984.

[18] Thomson, P. F., *An analysis of necking in axi-symmetric tension specimens*, International Journal of Mechanical Sciences, Vol. 11, pp. 481-490, 1969.

[19] Zhnag, K. S., Li, Z. H., *Numerical analysis of the stress-strain curve and fracture initiation for ductile material*, Engineering fracture mechanics, Vol. 49, pp. 235-241, 1994.

[20] Livermore Software Technology Corporation, *LS-Dyna Keyword User's Manual Volume I*, ver 971, rev.1433, Livermore 29 may 2012.

[21] Livermore Software Technology Corporation, *LS-Dyna Keyword User's Manual Volume II*, ver 971, rev.1437, Livermore 29 may 2012.